Neutrino production of opposite sign dimuons in the NOMAD experiment

P. Astier [o], D. Autiero [i], A. Baldisseri [s], M. Baldo-Ceolin [n], G. Ballocchi [i],
M. Banner [o], G. Bassompierre [a], K. Benslama [j], N. Besson [s], I. Bird [j,i],
B. Blumenfeld [b], F. Bobisut [n], J. Bouchez [s], S. Boyd [t], A. Bueno [c,x],
S. Bunyatov [g], L. Camilleri [i], A. Cardini [k], P.W. Cattaneo [p], V. Cavasinni [q],
A. Cervera-Villanueva [i,w], G.M. Collazuol [n], G. Conforto [i,u], C. Conta [p],
M. Contalbrigo [n], R. Cousins [k], D. Daniels [c], H. Degaudenzi [j], A. De Santo [i,q],
T. Del Prete [q], T. Dignan [c], L. Di Lella [i], E. do Couto e Silva [i],
J. Dumarchez [o], M. Ellis [t], T. Fazio [a], G.J. Feldman [c], R. Ferrari [p],
D. Ferrère [i], V. Flaminio [q], M. Fraternali [p], J-M. Gaillard [a], E. Gangler [o],
A. Geiser [i,f], D. Geppert [f], D. Gibin [n], S. Gninenko [m], A. Godley [t],
J-J. Gomez-Cadenas [i,w], J. Gosset [s], C. Gößling [f], M. Gouanère [a], A. Grant [i],
G. Graziani [h], A. Guglielmi [n], C. Hagner [s], J. Hernando [w], D. Hubbard [c],
P. Hurst [c], N. Hyett [l], E. Iacopini [h], C. Joseph [j], F. Juget [j], M. Kirsanov [m,u],
O. Klimov [g], J. Kokkonen [i], A. Kovzelev [m,p], A. Krasnoperov [a,g],
V. Kuznetsov [g,i], S. Lacaprara [n], B. Lakic [v], A. Lanza [p], L. La Rotonda [e],
M. Laveder [n], A. Letessier-Selvon [o], J-M. Levy [o], L. Linssen [i], A. Ljubičić [v],
J. Long [b], A. Lupi [h], E. Manola-Poggioli [a], A. Marchionni [h], F. Martelli [u],
X. Méchain [s], J-P. Mendiburu [a], J-P. Meyer [s], M. Mezzetto [n], S.R. Mishra [c,d],
G.F. Moorhead [l], L. Mossuz [a], P. Nédélec [a], Yu. Nefedov [g], C. Nguyen-Mau [j],
D. Orestano [r], F. Pastore [r], L.S. Peak [t], E. Pennacchio [u], H. Pessard [a],
R. Petti [p], A. Placci [i], A. Pluquet [s], G. Polesello [p], D. Pollmann [f], A. Polyarush [m],
B. Popov [g,o], C. Poulsen [l], P. Rathouit [s], C. Roda [i,q], A. Rubbia [i,x], F. Salvatore [p],
K. Schahmaneche [o], B. Schmidt [f,i], T. Schmidt [f], M.E. Sevior [l], D. Sillou [a],
F.J.P. Soler [t,i], G. Sozzi [j], D. Steele [b,j], M. Steininger [j], U. Stiegler [i], M. Stipčević [v],
T. Stolarczyk [s], M. Tareb-Reyes [j], G.N. Taylor [l], S. Tereshchenko [g], A. Toropin [m],
A-M. Touchard [o], S.N. Tovey [i,l], M-T. Tran [j], E. Tsesmelis [i], J. Ulrichs [t],
L. Vacavant [j], M. Valdata-Nappi [e], V. Valuev [g,k], F. Vannucci [o], K.E. Varvell [t],
M. Veltri [u], V. Vercesi [p], D. Verkindt [a], J-M. Vieira [j], T. Vinogradova [k],

M-K. Vo [s], F. Weber [c,i], T. Weisse [f], F. Wilson [i], L.J. Winton [l], B.D. Yabsley [t], H. Zaccone [s], K. Zuber [f], P. Zuccon [n]

[a] *LAPP, Annecy, France*
[b] *Johns Hopkins University, Baltimore, MD, USA*
[c] *Harvard University, Cambridge, MA, USA*
[d] *University of South Carolina, Columbia, SC, USA*
[e] *University of Calabria and INFN, Cosenza, Italy*
[f] *Dortmund University, Dortmund, Germany*
[g] *JINR, Dubna, Russia*
[h] *University of Florence and INFN, Florence, Italy*
[i] *CERN, Geneva, Switzerland*
[j] *University of Lausanne, Lausanne, Switzerland*
[k] *UCLA, Los Angeles, CA, USA*
[l] *University of Melbourne, Melbourne, Australia*
[m] *Institute for Nuclear Research, INR Moscow, Russia*
[n] *University of Padova and INFN, Padova, Italy*
[o] *LPNHE, University of Paris, Paris VI and VII, Paris, France*
[p] *University of Pavia and INFN, Pavia, Italy*
[q] *University of Pisa and INFN, Pisa, Italy*
[r] *Roma-III University, Rome, Italy*
[s] *DAPNIA, CEA Saclay, Saclay, France*
[t] *University of Sydney, Sydney, Australia*
[u] *University of Urbino, Urbino, and INFN, Florence, Italy*
[v] *Rudjer Bošković Institute, Zagreb, Croatia*
[w] *IFIC, Valencia, Spain*
[x] *ETH Zürich, Zürich, Switzerland*

Abstract

The NOMAD Collaboration presents a study of opposite sign dimuon events in the framework of Leading Order QCD. A total of 2714 neutrino- and 115 antineutrino-induced opposite sign dimuon events with $E_{\mu 1}, E_{\mu 2} > 4.5$ GeV, $15 < E_\nu < 300$ GeV and $Q^2 > 1\,(\text{GeV}/c)^2$ are observed in the Front-Calorimeter of NOMAD during the 1995 and 1996 runs. The analysis yields a value for the charm quark mass of $m_c = 1.3^{+0.3+0.3}_{-0.3-0.3}$ GeV/c^2 and for the average semileptonic branching ratio of $B_c = 0.095^{+0.007+0.014}_{-0.007-0.013}$. The ratio of the strange to non-strange sea in the nucleon is measured to be $\kappa = 0.48^{+0.09+0.17}_{-0.07-0.12}$. The measured rate of charm-induced dimuon relative to single muon, as a function of neutrino energy, is consistent with the slow rescaling hypothesis of heavy quark production. © 2000 Published by Elsevier Science B.V.

1. Introduction

A charged current muon-neutrino deep inelastic scattering event produces a single muon at the leptonic vertex and changes the flavour of the initial quark at the hadronic vertex. If the initial quark is a strange (down) quark, a charm quark may be produced via a Cabibbo enhanced (suppressed) transition. The charm quark then fragments into a charmed hadron which may decay semileptonically, producing either a second muon or an electron with its electric charge opposite to that of the muon from the leptonic vertex. This type of event is referred to as an opposite sign dilepton event. If the second lepton is a muon the event is usually labelled as a dimuon event. This process is a powerful and clean probe of both the strange component of the nucleon sea and the kinematics of heavy quark production.

E-mail address: mishra@axnd02.cern.ch (S.R. Mishra).

The phenomenon of charm production by neutrinos has been investigated by a number of experiments. Dimuons have been studied in counter experiments: CDHS [1], CHARM II [4], CCFR [3] and FMMF [5]; in bubble chamber experiments such as Col-BNL [6], BEBC [7] and E362 [8] at Fermilab; and in the Fermilab emulsion experiments, E531 [9] and E564 [10]. Bubble chamber experiments generally have too few events to study the parameters of charm production with any precision. It is the counter experiments, and the E531 experiment, which have provided much of our knowledge of neutrino charm production.

This paper presents the results of an analysis of opposite sign dimuon events carried out by the NO-MAD collaboration. The distributions of various kinematic variables are compared with a theoretical model of dimuon production, constructed within the framework of leading order QCD, to yield a determination of the charm quark mass, m_c, the strange quark fraction of the nucleon sea, κ, and the average semileptonic branching ratio, B_c. The paper is organised as follows: Section 2 outlines the theoretical description of opposite sign dimuon production within the framework of leading order QCD and Section 3 gives a brief description of the neutrino beam. The detector is described in Section 4 along with a description of the simulation programs used in the analysis (Section 4.2), a description of the data selection process and a discussion of the background determination. Section 5 presents details of the analysis and Section 6 contains a discussion and a comparison with the results of other experiments. Finally, Section 7 summarizes the results.

2. Theory

In the Standard Model, an opposite sign dimuon event is produced when a neutrino interacts, via a charged current, with a strange (s) or down (d) quark, producing a charm (c) quark. The charm quark fragments into a charmed hadron (most frequently a D meson) which can then decay semileptonically resulting in a final state containing two oppositely charged muons: the *primary* muon which comes from the leptonic vertex and the *secondary* muon which arises from the decay of the charmed hadron.

The large mass of the charm quark, m_c, gives rise to an energy threshold which has the effect of suppressing the opposite sign dimuon production rate at low neutrino energies. This is effectively described by the slow rescaling model [11] in which the usual scaling variable, $x = Q^2/2M\nu$, is replaced by the slow-rescaling variable, $\xi = x(1 + m_c^2/Q^2)$. With this replacement, the leading order cross section for opposite sign dimuon production by neutrino scattering on an isoscalar target may be written [5]

$$
\frac{d^3\sigma^\nu}{d\xi\,dy\,dz} = \frac{G_F^2 M E_\nu \xi}{\pi}
$$

$$
\times \left\{ \left[u(\xi, Q^2) + d(\xi, Q^2) \right] |V_{cd}|^2 \right.
$$

$$
\left. + 2s(\xi, Q^2)|V_{cs}|^2 \right\}
$$

$$
\times \left(1 - y + \frac{xy}{\xi} \right) D(z) B_c \tag{1}
$$

where G_F is the Fermi constant; E_ν is the energy of the incident neutrino; M is the mass of the nucleon; Q^2 is the negative four momentum transfer squared; x and y are the Bjorken variables; z is defined to be the ratio of the momentum of the charmed hadron to the maximum momentum that the kinematics will allow that hadron to possess; V_{cd} and V_{cs} are Cabibbo–Kobayashi–Maskawa (CKM) matrix elements [12] and $u(\xi, Q^2)$, $d(\xi, Q^2)$ and $s(\xi, Q^2)$ are the up, down and strange quark structure functions, respectively. The function $D(z)$, discussed below in Section 4.2, describes the fragmentation of the charm quark into a charmed hadron and B_c is the average semileptonic branching ratio for charmed hadron decay. The corresponding cross section for incident antineutrinos is obtained by replacing the quark structure functions with the antiquark structure functions in Eq. (1). It should be noted that the slow rescaling hypothesis is an effective – and, as demonstrated by our data, consistent – description of the heavy quark production. A next-to-leading (NLO) order treatment of the data would yield different values for the structure function related parameters [2].

3. Neutrino beam

The CERN-SPS wide band beam is produced by 450 GeV/c protons incident on a beryllium target. The secondary pions and kaons pass through a large angle aluminium collimator and are focussed by a system of magnetic lenses, which focus(defocus) positive(negative) mesons. The particles decay in a 290 m long evacuated decay tunnel and the decay products then pass through an earth and iron shield which filters out all but the neutrinos and some muons. Monte Carlo predictions of the relative beam composition and average energies of various neutrino types present in the beam are summarised in Table 1 [13]. Variations in the relative beam compositions were used to estimate the systematic uncertainty due to the beam description in the parameters determined in Section 5.

4. Experimental details

4.1. Apparatus

The NOMAD detector, designed to search for a neutrino oscillation signal in the CERN SPS wide band neutrino beam, is described in detail in Ref. [14]. A side view of the detector is shown in Fig. 1. It consists of a number of subdetectors, most of which are located inside a 0.4 T dipole magnet with a volume of $7.5 \times 3.5 \times 3.5 \, \text{m}^3$. The relevant features for the present study will be briefly mentioned.

An iron-scintillator hadronic calorimeter, denoted the Front Calorimeter (FCAL), located upstream of the central part of the NOMAD detector, forms the target for the opposite sign dimuon study. It consists of 23 iron plates, 4.9 cm thick, separated by 1.8 cm air gaps. The first 20 gaps are instrumented with long scintillators which are read out at both ends by 3 in. photomultipliers. The dimensions of the scintillators are $175 \times 18.5 \times 0.6 \, \text{cm}^3$ and five consecutive scintillators are ganged together to form a module. Ten such modules are placed on top of one another to form a stack and there are four stacks aligned along the beam axis. The total instrumented region has a mass of 17.7 t and is about 5 nuclear interaction lengths thick. The energy scale of the FCAL

Table 1
Average energies and relative abundances of neutrino types in the CERN-SPS wide band beam

	Average E_ν (GeV)	Relative flux abundance
ν_μ	23.5	1.000
$\bar{\nu}_\mu$	19.2	0.061
ν_e	37.1	0.0094
$\bar{\nu}_e$	31.3	0.0024

was calibrated in two stages. The relative calibration stage used high energy muons to derive the response of each FCAL module to the energy deposited by a minimum ionising particle (mip). The absolute energy scale, derived from a Monte Carlo study of neutral current neutrino interactions in which all the hadronic energy was contained within the FCAL volume, was then used to convert the energy deposition in units of mips to units of GeV. The energy calibration factor was determined to be $(2.95 \pm 0.02) \, \text{mip/GeV}$. Using this calibration factor the energy resolution of the FCAL is $\sigma/E = 100\%/\sqrt{E \, (\text{GeV})}$ [15].

The tracking detector consists of 44 drift chambers grouped into 11 modules. This is followed by a transition radiation detector (TRD) to enhance the separation of electrons from pions. Five additional drift chambers are interleaved with the TRD modules. A preshower (PRS) detector precedes an electromagnetic calorimeter (ECAL), which consists of an array of lead glass Čerenkov counters. The energy resolution of the ECAL is $\sigma/E = 1\% + 3.2\%/\sqrt{E(\text{GeV})}$ [14].

A hadronic calorimeter (HCAL) with an energy resolution of $\sigma/E = 100\%/\sqrt{E(\text{GeV})}$ is installed behind the magnet coil and is followed by two muon detection stations consisting of large area drift chambers, the first after 8 and the second after 13 nuclear interaction lengths.

The FCAL trigger signal is obtained as the logical OR of the signals from each stack. A plane of scintillators, V_8, mounted on the upstream face of the FCAL as part of the veto, rejects charged particles either in the beam or from interactions in material upstream of NOMAD. Neutrino interactions in the FCAL are selected by a $\overline{V_8} \times FCAL$ trigger with a threshold set at 75 mV, corresponding to a deposited energy of approximately 2.0 GeV. The average rate
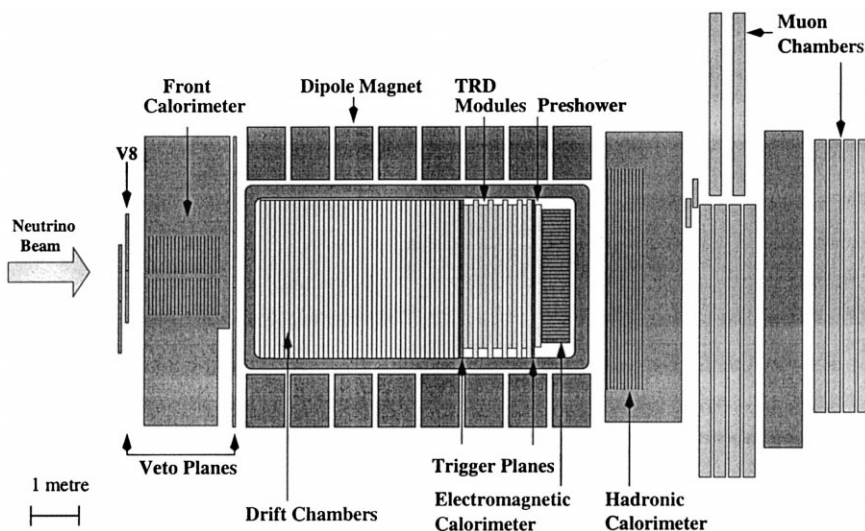
Fig. 1. Side view of the NOMAD detector. The coordinate system has the x-axis into the plane of the figure, the y-axis directed up towards the top of the figure and the z-axis horizontal, approximately along the direction of the neutrino beam (which points upwards at an angle of 2.4° with respect to the z-axis).

of the $\overline{V_8} \times FCAL$ trigger is 6.5 per 10^{13} protons on target (p.o.t), with negligible cosmic ray background. The trigger livetime is $(89.5 \pm 2.2)\%$ [16].

4.2. Monte Carlo simulations

The opposite sign dimuon study reported here utilised two detector simulations. The first was a GEANT [17] based full detector simulation which included a detailed description of the detector geometry and which simulated the response of the detector to the particles produced in neutrino interactions. Neutrino events were simulated using a deep inelastic scattering event generator based on the LEPTO 6.1 [18] and JETSET 7.4 [19] packages. These events were then passed through the GEANT simulation and reconstructed in the same way as data. The full scale simulation was, however, too slow to use for the analysis presented in Section 5. To overcome this problem a fast detector simulation was constructed [15]. This simulation used detector response functions derived from the detailed simulation to model the detector acceptance, resolution and smearing, the efficiency of event selection and the details of the physics of both opposite sign dimuon and single muon charged current events. The parton densities used were those measured by the CCFR experiment

[2]. These parton densities were found to reproduce well the shape of the kinematic distributions of the single muon NOMAD data [15]. Non-isoscalarity of the target and the violation of the Callan–Gross relation were included.

The fragmentation of the charm quark into a charmed hadron was modelled using the Collins–Spiller fragmentation function [20], which has been shown to describe adequately charm fragmentation data from the e^+e^- experiment CLEO [21,22]. This function is parametrised by

$$D(z) = N_0 \left(\frac{1-z}{z} + \frac{\epsilon_C(2-z)}{1-z} \right)(1+z^2)$$

$$\times \left(1 - \frac{1}{z} - \frac{\epsilon_C}{1-z} \right)^{-2} \qquad (2)$$

where $z = p_h / p_h^{max}$ is the ratio of the momentum of the charmed hadron to the maximum momentum that the kinematics will permit that charmed hadron to possess, N_0 is a normalisation factor that ensures that the integral of $D(z)$ is unity and ϵ_C is a free parameter which has been determined by CLEO [22] to be (0.6 ± 0.1) and by CCFR [23] to be (0.8 ± 0.2). This study uses a value of $\epsilon_C = 0.64 \pm 0.09$, the weighted average of the CLEO and CCFR results.

During fragmentation the charmed hadron acquires a momentum component transverse to the original direction of the charm quark. The size of this transverse component, p_T, was parametrised as $dN/dp_T^2 \propto e^{-\beta p_T^2}$ where p_T is in units of GeV/c. The value of the parameter β was taken to be $1.1 \pm 0.3\,(\text{GeV}/\text{c})^{-2}$, as measured by the LEBC collaboration [24].

To model the relative proportion of charmed hadron species, we used the most recent analysis of the E531 [9] data as quoted in Ref. [2]. In that analysis, the production fractions of charmed hadrons were determined to be $(60 \pm 6)\%$ D^0, $(26 \pm 6)\%$ D^+, $(7 \pm 5)\%$ D_s^+ and $(7 \pm 4)\%$ Λ_c^+ over a neutrino energy range of 30 GeV to 200 GeV. The neutrino energy spectrum at NOMAD extends below 30 GeV, so to guard against systematic error a second analysis was performed using different production fractions, obtained from an earlier E531 analysis [25], in the range $E_\nu < 30$ GeV. The effect on the final result was negligible.

The branching ratios of the different semileptonic decay modes of the D meson and the Λ_c baryon are listed in Table 2 [12]. The D meson was decayed using a spin-1 vector matrix element in the case of the K^* decay mode and a spin-0 pseudoscalar matrix element for the other decays [26]. As in JETSET [19], the decay of the Λ_c baryon was carried out using a V-A matrix element to distribute the decay products.

4.3. Data sample and event selection

The present analysis is based on data collected during the 1995 and 1996 NOMAD runs. The total exposure was 1.8×10^{19} p.o.t. Candidate opposite sign dimuon events were selected by the following criteria:

· Two muons of opposite electric charge had to be identified.
· The approximate longitudinal vertex position, identified as the midplane of the first stack in which there was significant energy deposition, must have occurred in one of the three most upstream stacks. The hadronic showers of events occurring in the last (fourth) stack are generally not longitudinally contained within the calorimeter and as a result the reconstructed properties of these events differ markedly from those events originating in the first three stacks.
· The transverse position of the vertex, obtained from energy sharing between the two ends of each module, had to be within the bounds of $-70\,\text{cm} < x < 70\,\text{cm}$ and $-70\,\text{cm} < y < 70\,\text{cm}$. This ensured that the hadronic shower was laterally contained.
· The distance between the positions of the muons, when extrapolated to the midplane of the first stack hit, had to be less than 20 cm.
· The difference between the fitted times of each muon track at the first hit in the drift chambers had to be less than 5 ns.

The dimuon events were categorised as originating from an incident neutrino or antineutrino by assuming that the primary muon (the muon produced at the leptonic vertex) was the one with the largest transverse momentum with respect to the beam direction. Monte Carlo studies indicate that this procedure identifies the correct primary muon with an efficiency of $(95 \pm 1)\%$ in neutrino induced interactions and $(93 \pm 1)\%$ in antineutrino interactions.

Denoting the 3-momentum and energy of the primary muon by $\mathbf{p}_1$ and E_1 respectively, the 3-momentum and energy of the secondary muon by $\mathbf{p}_2$ and E_2, the energy measured by the FCAL (the visible hadronic energy) by $E_{\text{vis}}^{\text{had}}$ and letting $\hat{\mathbf{a}}$ represent a unit vector parallel to the beam direction, we may define the following kinematic quantities:

· $E_{\text{vis}}^\nu = E_1 + E_2 + E_{\text{vis}}^{\text{had}}$, the visible neutrino energy;

Table 2
The branching ratio of D meson and Λ_c baryon semileptonic decays relative to their respective total muon semileptonic branching fraction

Mode	Relative branching ratio
$D \to \nu\mu\pi$	0.05
$D \to \nu\mu K$	0.67
$D \to \nu\mu K^*$	0.28
$\Lambda_c \to \Lambda\nu\mu$	0.49

- $Q_{\mathrm{vis}}^2 = 2 E_{\mathrm{vis}}^{\nu}(E_1 - \mathbf{p_1} \cdot \hat{\mathbf{a}}) - m_{\mu}^2$, the visible negative four-momentum transfer squared;
- $\nu_{\mathrm{vis}} = E_2 + E_{\mathrm{vis}}^{\mathrm{had}}$, the visible energy transferred to the hadronic system.
- $x_{\mathrm{vis}} = Q_{\mathrm{vis}}^2 / 2M\nu_{\mathrm{vis}}$, the visible Bjorken x;
- $y_{\mathrm{vis}} = \nu_{\mathrm{vis}} / E_{\mathrm{vis}}^{\nu}$, the visible Bjorken y;

In addition to the topological cuts listed earlier, a set of kinematic cuts were also applied. Both muons were required to have an energy greater than 4.5 GeV, primarily to reduce the meson decay background. The visible hadronic energy, $E_{\mathrm{vis}}^{\mathrm{had}}$, was required to be more than 5 GeV to ensure good hadronic energy reconstruction. Finally, badly reconstructed events (e.g. events in which the energy of the primary muon was too high to measure accurately) and events in regions where the simulation was considered to be unreliable were rejected by the criteria $x_{\mathrm{vis}} < 1$ and $Q_{\mathrm{vis}}^2 > 1\,\mathrm{GeV}^2$.

From a Monte Carlo simulation using the above criteria, the dimuon selection efficiency was estimated to be $(14 \pm 2)\%$. The largest loss of efficiency was due to the requirement that the secondary muon be identified as a muon. The average momentum of the secondary muon is approximately 5 GeV/c. Requiring that it be observed in the muon chambers imposes an implicit momentum cut of at least 3 GeV/c, due to the rangeout of the muons within the

FCAL itself or in the rest of the detector. This requirement, coupled with the steep secondary muon momentum spectrum, leads to a significant loss of events.

Fig. 2 shows an example dimuon event from the NOMAD data.

4.4. Background estimation

The background to the opposite sign dimuon process arises from muonic decays of hadrons produced in the hadronic shower or by hadrons which punch through to the muon chambers, thereby simulating muons. The amount of background was estimated by studying dimuon events in which both muons had identical electric charge, the so-called like sign events. This class of events is dominated by the decay of hadrons (mostly pions and kaons) [27,28] and hence, since the same physics processes give rise to the like sign events as to the opposite sign background events, can be used to estimate the background to the opposite sign dimuon signal.

The background subtraction algorithm, for any distribution **A** under study, was as follows:

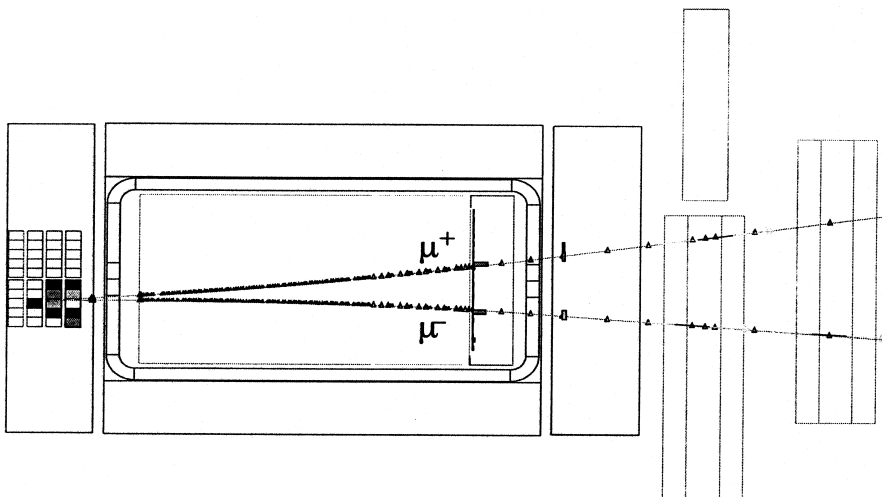- the number of like sign events in the data was determined.

Fig. 2. Example of an opposite sign dimuon event occurring at the end of Stack 2 in the FCAL. The two tracks are the oppositely charged muons in the event and the detector is shown from the side. The grey shading in each FCAL module indicates different levels of energy deposition.

Table 3
The number of reconstructed opposite sign background events, like sign events and their ratio in simulated neutrino and antineutrino charged current event samples

	ν_μ	$\bar{\nu}_\mu$
initial number of events	288,000	72,144
number of non-charm opposite sign background events	61 ± 8	10 ± 3
number of like sign events	40 ± 6	5 ± 2
background scale, **R**	1.5 ± 0.3	2^{+2}_{-1}

- using the detailed Monte Carlo, the ratio, **R**, of the number of reconstructed opposite sign background events to the number of reconstructed like sign events was calculated. Due to a combination of leading charge effects and slightly different acceptances for positive and negative muons, more opposite sign background events were observed than like sign events. This is illustrated in Table 3.
- the same distribution for the like sign events in the data, $\mathbf{A}^{\mathrm{LSDM}}_{\mathrm{DATA}}$, was scaled by **R**.
- the scaled distribution was subtracted, bin-by-bin, from **A**.

For this prescription to be valid it is important that the simulation describes both the shapes of the distributions of the like sign data and the production rate satisfactorily. The rate of observed like sign events normalised to the number of observed neutrino charged current events was measured to be $(2.7 \pm$
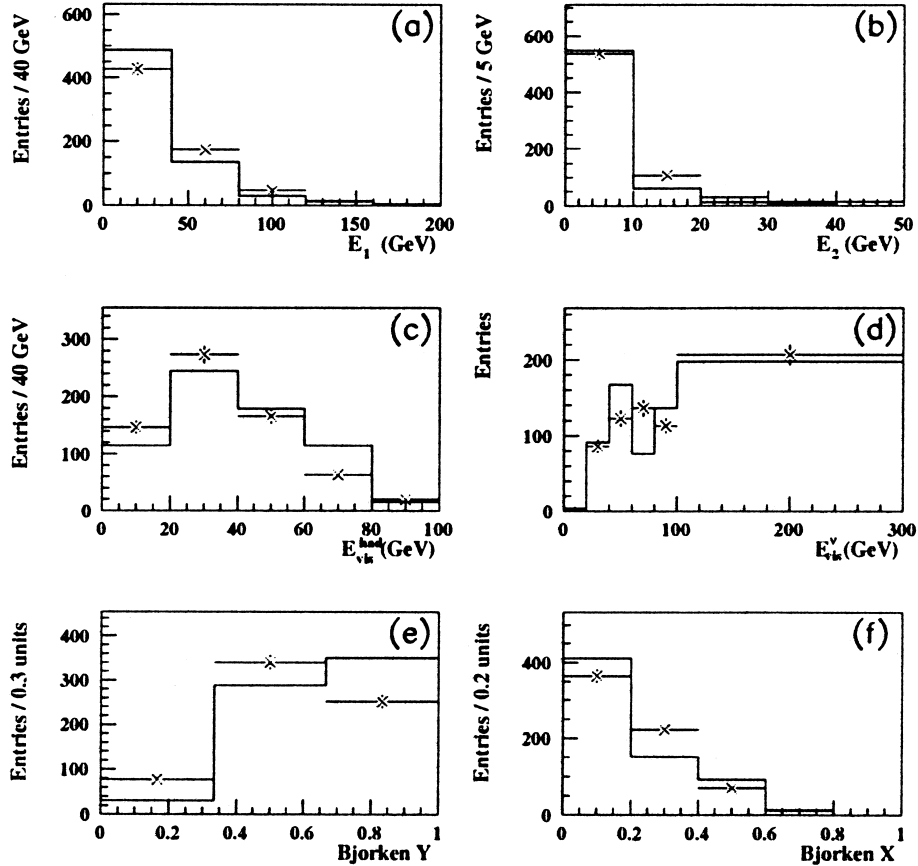

Fig. 3. Comparison of the shapes of the kinematic distributions of like sign dimuon simulation (histogram) and data (points). Shown are the distributions of (a) the energy of the primary muon, (b) the energy of the secondary muon candidate, (c) the visible hadronic energy, (d) the visible neutrino energy, (e) Bjorken y and (f) Bjorken x. The distributions from the data and simulation have been normalised to equal area.

Table 4

The number of events with a leading μ^- or μ^+. Shown are the total number of opposite sign events observed, the total number of like sign events, the background estimate and the number of opposite sign events from charm production corrected for background and contamination of the neutrino(antineutrino) sample by the antineutrino (neutrino) sample. The background is estimated by scaling the number of like sign events by 1.5 ± 0.3 for the neutrino induced dimuons and by $2.0^{+2.0}_{-1.0}$ for the antineutrino sample. The uncertainty on the number of corrected events combines the statistical error on the raw opposite sign and like sign dimuon event numbers with the uncertainty on the background scaling factor and the errors on the neutrino and antineutrino dimuon event recognition efficiencies

	Leading μ^-	Leading μ^+
number of opposite sign events in data	3590	259
like sign events in data	669	8
estimated number of opposite sign background events	1004	16
number of opposite sign dimuon events after background subtraction and correction for cross-contamination	2714 ± 227	115^{+38}_{-41}

$0.1) \times 10^{-4}$ in the data, to be compared to $(2.7 \pm 0.4) \times 10^{-4}$ in the detailed simulation. Fig. 3 shows a comparison of the shapes of various distributions of like sign events in the data and the simulation. The agreement is good.

Other background sources such as trident production [29,30], the overlap of a neutrino and an antineutrino event, or the production and subsequent muonic decay of a J/ψ were found to be negligible in this analysis.

A total of 3590 leading μ^- and 259 leading μ^+ events survived the selection process. Subtracting the background and correcting for contamination of the neutrino sample by antineutrino-induced dimuon events (and vice versa) yields an estimated number of 2714 neutrino-induced and 115 antineutrino-induced dimuon events. Table 4 summarizes the number of dimuon events in the data sample.

5. Analysis

5.1. Description and results

The production of opposite sign dimuon events is governed by four parameters: the charm quark mass, m_c, the proportion of strange to nonstrange quarks in the nucleon sea, usually determined by the parameter $\kappa = 2\bar{S}/(\bar{U} + \bar{D})$ (where $\bar{S} = \int_0^1 x\bar{s}(x)dx$, $\bar{U} = \int_0^1 x\bar{u}(x)dx$ and $\bar{D} = \int_0^1 x\bar{d}(x)dx$), the CKM matrix element, V_{cd}^1, and B_c, the average semileptonic

---

[1] The CKM element, V_{cs}, can be obtained from the unitarity condition of the CKM matrix.

branching ratio of charmed hadrons. Determinations of these parameters were made by fitting the observed kinematic distributions to model distributions obtained from a Monte Carlo simulation. To obtain the model predictions for different sets of production parameters, each simulated event in a ''seed'' event sample was given a weight proportional to the ratio of the differential cross sections for that event, calculated using the parameters for the new and seed samples. The seed sample consisted of approximately 140,000 neutrino dimuon events (after event selection) generated with $m_c = 0.1\,\mathrm{GeV}/c^2$, $\kappa = 0.36$, $V_{cs} = 0.974$ [12] and $V_{cd} = 0.221$ [12] using the fast Monte Carlo code described in Section 4.2. The charm quark mass at generation was chosen to be small to ensure that the fit was not biased by any mass thresholds in the seed sample.

Since the antineutrino sample was only a small fraction of the total event sample, it was expected that any determination of V_{cd} would be less precise than the current value of (0.221 ± 0.003) and so V_{cd} and V_{cs} were fixed to their best known values.

A simultaneous fit for m_c and κ was performed using MINUIT [31] in order to check the degree of correlation between the two variables. The correlation was found to be small, allowing each parameter to be determined independently of the other. The mass of the charm quark was estimated by analysing the shape of the E^ν_{vis} distribution after selection cuts had been applied, with κ held constant. Once m_c was determined, κ was measured using the shape of the x_{vis} distribution. Finally, the average semileptonic branching ratio, B_c, was extracted by studying

Table 5

Fit results, statistical and systematic uncertainties and the fit χ^2/d.o.f (degree of freedom) for parameters of the dimuon cross section

Parameter	Result	Statistical uncertainty	Systematic uncertainty	Fit χ^2 per d.o.f
m_c	1.3	$+0.3 \atop -0.3$	$+0.3 \atop -0.3$	6.1/5
κ	0.48	$+0.09 \atop -0.07$	$+0.17 \atop -0.12$	3.3/4
B_c	0.095	$+0.007 \atop -0.007$	$+0.014 \atop -0.013$	–

the observed rate of dimuons with respect to single muon events. The optimum value of each parameter was determined by a χ^2 minimization procedure. The E_{vis}^{ν} distribution was split into 6 bins (0 – 20 – 30 – 50 – 80 – 100 – 300 GeV) and the x_{vis} distribution was split into 5 bins (0 – 0.05 – 0.1 – 0.3 – 0.5 – 1.0). The bins were defined so that the statistical uncertainty in each bin was approximately equal. Table 5 shows the fit results along with the statistical and systematic uncertainties on each parameter and the χ^2 for each fit. The systematic uncertainties are discussed below. A comparison of distributions from a Monte Carlo sample generated with the best fit values of m_c and κ and data is shown in Fig. 4. The good agreement shows that the slow-rescaling model of charm quark production by neutrinos describes the data well.

5.2. Systematic errors

Systematic errors on the fit results arise from uncertainties in the theoretical model, uncertainties in the exact value of reconstructed kinematic variables which define the analysis cuts and uncertainties in the background subtraction procedure. The theoretical uncertainties were studied by varying the parameters of the model by their quoted errors, repeating the fit, and observing the shift in the best fit values of m_c, κ and B_c. The effect of the finite resolution on the cut variables was studied by varying each cut around its central value and repeating the fit. The systematic uncertainty due to the background scale was estimated by varying the scale within its errors (see Table 3). The parton densities used in this analysis were based on the Buras–Gaemers model with nine free parameters [2,32]. The impact of the uncertainties in these distribution functions on the charm parameters was studied by varying each of the nine parameters by their quoted error and repeating the fit. The uncertainty due to the

beam description was estimated by weighting the seed sample events by the ratio of the flux predictions from two different beam descriptions and repeating the analysis. One beam description uses a version of FLUKA which is incorporated into the GEANT [17] package and was the default simulation for this analysis. The other beam simulation (the so called *empirical parametrisation*) uses cross sections for meson and hadron production in ν-Be interactions which have been determined from the analysis of ν_{μ}, $\bar{\nu}_{\mu}$, ν_e and $\bar{\nu}_e$ energy spectra observed in the NOMAD data and which agree with empirically measured production yields [33].

A summary of the systematic errors is presented in Table 6. The effect of varying the value of the cut on Bjorken x was negligible in all cases.

6. Discussion

A comparison of these results with those reported by the CDHS [1], CHARM II [4], CCFR [3] and FMMF [5] experiments is shown in Table 7. All parameters measured in this study are compatible with previous experiments.

Within the framework of leading order QCD, an SU(3) symmetric sea would yield a value of $\kappa = 1$. The smaller value observed supports the conclusion that the size of the strange sea is suppressed with respect to the size of the non-strange sea. The strange sea content of the nucleon may be defined by $\eta_s = 2 S/(U + D)$. Using the measured value of κ and taking the total antiquark to quark ratio, $\bar{Q}/Q$, to be 0.177 from the CCFR [3] parton density parametrisation yields

$$\eta_s = 0.071^{+0.011+0.020}_{-0.009-0.015} \qquad (3)$$

which is consistent with previous publications [3,4]. The average branching ratio determined in this study
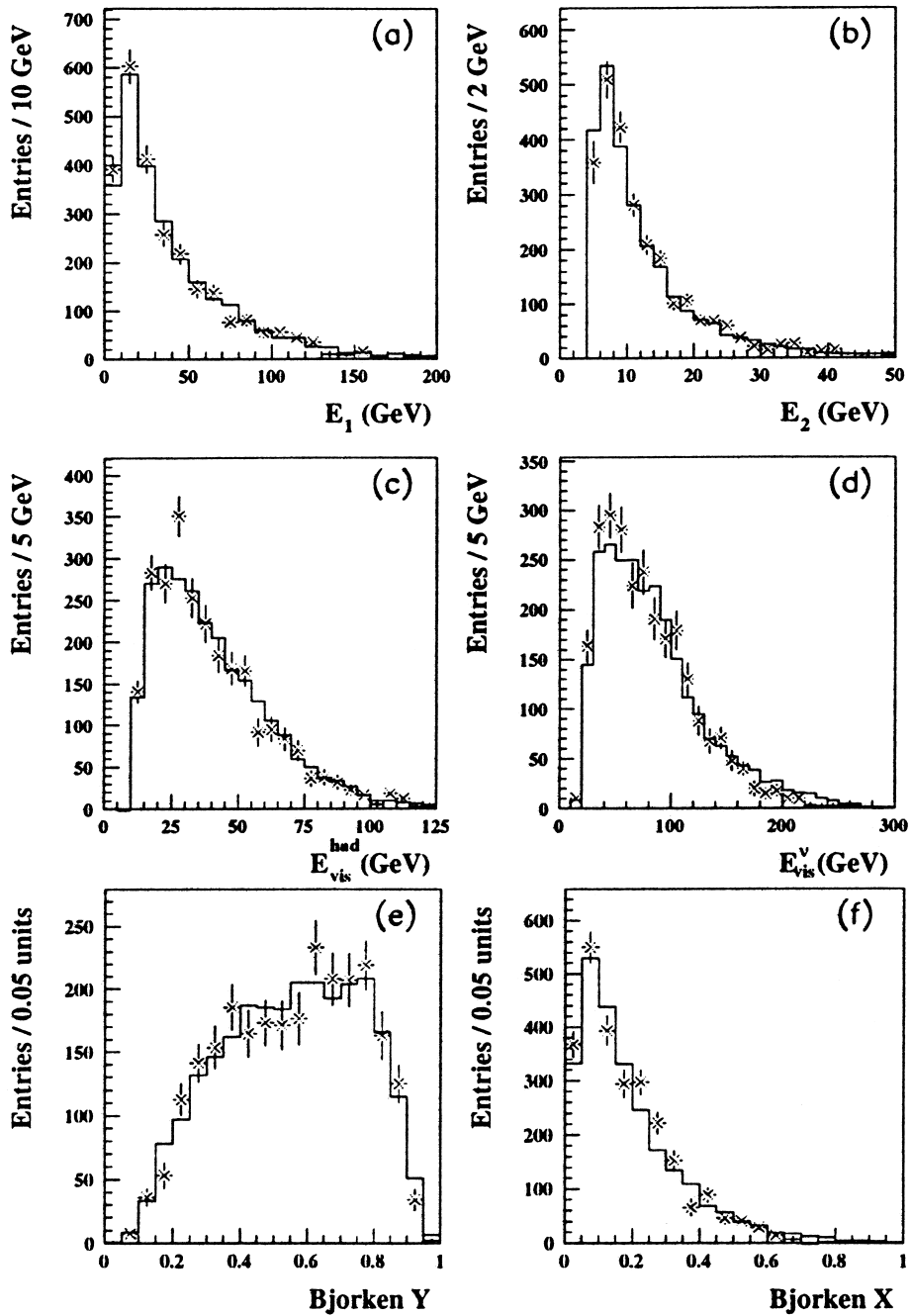
Fig. 4. Comparison of the shapes of the kinematic distributions of an opposite sign dimuon simulation (histogram) and background subtracted data (points). Shown are distributions of (a) the energy of the primary muon, (b) the energy of the secondary muon, (c) the visible hadronic energy, (d) the visible neutrino energy, (e) visible Bjorken y and (f) visible Bjorken x. The distributions from the data and simulation have been normalised to equal area.

Table 6
Contributions to the total systematic uncertainties in the fitted parameters

Source of uncertainty	Δm_c	$\Delta\kappa$	ΔB_c
Theoretical Uncertainties			
background scale	$^{+0.16}_{-0.17}$	$^{+0.10}_{-0.06}$	$^{+0.0070}_{-0.0080}$
fragmentation parameter	$^{+0.03}_{-0.04}$	$^{+0.005}_{-0.003}$	$^{+0.0011}_{-0.0023}$
p_T distribution (β)	$^{+0.03}_{-0.02}$	$^{+0.004}_{-0.007}$	$^{+0.0013}_{-0.0005}$
m_c	-	$^{+0.07}_{-0.05}$	$^{+0.002}_{-0.003}$
κ	$^{+0.07}_{-0.03}$	-	$^{+0.012}_{-0.0095}$
V_{cd}	$^{+0.01}_{-0.01}$	$^{+0.05}_{-0.02}$	$^{+0.0001}_{-0.0001}$
V_{cs}	$^{+0.01}_{-0.01}$	$^{+0.02}_{-0.01}$	$^{+0.0001}_{-0.0001}$
structure functions	±0.06	±0.02	±0.001
target mass correction	±0.11	±0.04	±0.002
radiative correction	±0.05	±0.05	±0.001
Experimental Uncertainties			
beam description	±0.01	±0.01	±0.0001
fiducial volume	$^{+0.02}_{-0.03}$	$^{+0.01}_{-0.01}$	$^{+0.0002}_{-0.0002}$
difference between fitted time of muons at first hit in drift chambers	$^{+0.01}_{-0.01}$	$^{+0.003}_{-0.001}$	$^{+0.0001}_{-0.0001}$
distance between muons at interaction point	$^{+0.05}_{-0.07}$	$^{+0.02}_{-0.02}$	$^{+0.0011}_{-0.0020}$
Q^2_{vis} cut	$^{+0.01}_{-0.03}$	$^{+0.01}_{-0.03}$	$^{+0.0003}_{-0.0008}$
$E^{\mathrm{had}}_{\mathrm{vis}}$ cut	$^{+0.09}_{-0.07}$	$^{+0.001}_{-0.004}$	$^{+0.0003}_{-0.0002}$
cut on energy of primary muon	$^{+0.04}_{-0.03}$	$^{+0.006}_{-0.006}$	$^{+0.0002}_{-0.0001}$
cut on energy of secondary muon	$^{+0.05}_{-0.03}$	$^{+0.004}_{-0.003}$	$^{+0.0009}_{-0.0008}$
background shape	$^{+0.06}_{-0.06}$	$^{+0.02}_{-0.03}$	-
hadronic energy scale	$^{+0.07}_{-0.04}$	$^{+0.08}_{-0.04}$	$^{+0.0003}_{-0.0006}$
total systematic uncertainty	$^{+0.27}_{-0.26}$	$^{+0.17}_{-0.12}$	$^{+0.014}_{-0.013}$

is compatible with the values obtained by other experiments (see Table 7).

The slow rescaling model may be best tested by investigating the rate of charm-induced dimuon production relative to single muon production as a function of neutrino energy. This relative rate is shown in Fig. 5. Data have been corrected bin-by-bin, using Monte Carlo simulation, for the effects of geometric acceptance, reconstruction efficiency, energy loss due to the charm decay neutrino and the energy resolution. The energy resolution correction takes into account the correlation between data points. The hadron energy scale is established by the measured single muons in the FCAL; the muon energy via the measured magnetic field in NOMAD. The statistical and systematic errors have been added in quadrature. The NOMAD data are compatible with the CCFR [3] and the CDHS [1] data, and extend to the crucial low neutrino energy region. The results clearly exhibit an energy dependence characteristic

Table 7
Comparison of CDHS, NOMAD, CHARM II, CCFR and FMMF Leading Order results. The experiments are listed from top to bottom in order of increasing average neutrino energy. Also shown are the numbers of neutrino- and antineutrino-induced opposite sign dimuon events observed by each experiment

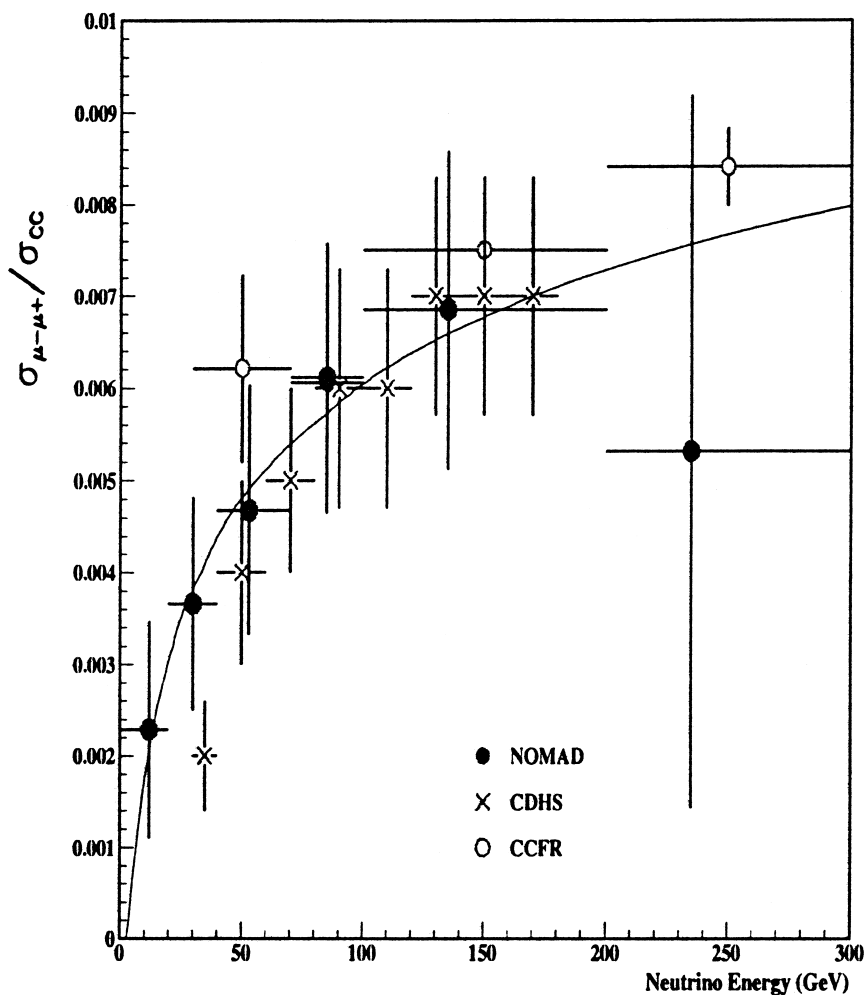| Experiment	$\langle E_{\nu_\mu}\rangle$	$N_{2\mu}$ for ν	$N_{2\mu}$ for $\bar\nu$	m_c (GeV/c^2)	κ	B_c
CDHS	20.0	9922	2123		$0.47^{+0.08+0.05}_{-0.08-0.05}$	$0.084^{+0.014}_{-0.014}$
NOMAD	23.6	2714	115	$1.3^{+0.3+0.3}_{-0.3-0.3}$	$0.48^{+0.09+0.17}_{-0.07-0.12}$	$0.095^{+0.007+0.014}_{-0.007-0.013}$
CHARM II	23.6	3100	700	$1.8^{+0.3+0.3}_{-0.3-0.3}$	$0.39^{+0.07+0.07}_{-0.06-0.07}$	$0.091^{+0.007+0.007}_{-0.007-0.007}$
CCFR	140.0	4503	632	$1.3^{+0.2+0.1}_{-0.2-0.1}$	$0.44^{+0.09+0.07}_{-0.07-0.02}$	$0.109^{+0.008+0.006}_{-0.008-0.006}$
FMMF		393			$0.41^{+0.08+0.103}_{-0.08-0.069}$	

Fig. 5. Neutrino-induced opposite sign dimuon rates corrected for acceptance and kinematic effects assuming a charm mass of 1.3 (GeV/c^2). The NOMAD results are displayed as closed circles. Also shown are the CCFR (open circles) and the CDHS results (crosses). The curve is the theoretical ratio of cross sections assuming the slow rescaling mechanism in Leading Order QCD, a charm mass of 1.3 (GeV/c^2), a value for κ of 0.48, an average semileptonic branching ratio of 0.095 and the validity of the CCFR structure functions.

of heavy quark production and are consistent with the slow-rescaling hypothesis. The measured charm excitation curve is the most precise to date in the energy region below 50 GeV.

7. Summary

Dimuon production by neutrinos in the NOMAD detector has been studied in the context of Leading Order QCD. The data are consistent with the hypoth-

esis of charm production via the slow rescaling model. Within this framework, the charm quark mass, $m_c = 1.3^{+0.3+0.3}_{-0.3-0.3}$ (GeV/c^2), and the strange content of the nucleon, $\eta_s = 0.071^{+0.011+0.020}_{-0.009-0.015}$, have been determined and shown to be compatible with the results of previous leading order QCD analyses. The strange quark content has been shown to be suppressed relative to the non-strange sea quarks by a factor of $\kappa = 0.48^{+0.09+0.17}_{-0.07-0.12}$. The average semileptonic branching ratio, determined to be $B_c = 0.095^{+0.007+0.014}_{-0.007-0.013}$, is consistent with the interpretation that it is a weakly rising function of neutrino energy,

arising from different energy dependencies of the various charmed hadron production rates.

References

[1] H. Abramowicz et al., Z. Phys. C 15 (1982) 19.
[2] A.O. Bazarko, Ph.D. thesis, Columbia University, 1994.
[3] CCFR Collaboration, S.A. Rabinowitz et al., Phys. Rev. Lett. 70 (1993) 134; CCFR Collaboration, C. Foudas et al., Phys. Rev. Lett. 64 (1990) 1207; CCFR Collaboration, A.O. Bazarko et al., Z. Phys. C 65 (1995) 189.
[4] P. Vilain et al., Eur. Phys. J. C 11 (1999) 19.
[5] B. Strongin et al., Phys. Rev. D 43 (1991) 2778.
[6] N.J. Baker et al., Phys. Rev. D 43 (1991) 2765.
[7] G. Gerbier et al., Z. Phys. C 29 (1985) 15.
[8] V. Jain et al., Phys. Rev. D 41 (1990) 2057.
[9] N. Ushida et al., Phys. Lett. B 121 (1983) 292.
[10] R.G. Ammar et al., Z. Phys. C 45 (1990) 557.
[11] H. Georgi, H.D. Politzer, Phys. Rev. D 14 (1976) 1829.
[12] Review of Particle Physics, Particle Data Group, Eur. Phys. J. C 3 (1998).
[13] G. Collazuol et al., CERN-OP EN-98–032 (1998).
[14] J. Altegoer et al., Nucl. Instrum. Methods A 404 (1998) 96.
[15] S. Boyd, Ph.D. thesis, University of Sydney, 1998.
[16] J. Altegoer et al., Nucl. Instrum. Methods A 428 (1999) 299.
[17] The NOMAD simulation program is based on GEANT 3.21, CERN Program Library Long Writeup W5013.
[18] G. Ingelman, in: Proc. Physics at HERA, 1992, W. Buchmueller, G. Ingelman (Eds.), DESY, Hamburg, 1992, p. 1366.
[19] T. Sjöstrand, Comput. Phys. Comm. 82 (1994) 74; CERN-TH/93–7112 (1993).
[20] P. Collins, T. Spiller, J. Phys. G 11 (1985) 1289.
[21] D. Andrews et al., Nucl. Instrum Methods A 211 (1983) 47.
[22] D. Bortoletto et al., Phys. Rev. D 37 (1988) 1719.
[23] A.O. Bazarko et al., Z. Phys. C 65 (1995) 189.
[24] M. Aguilar-Benitez et. al., Phys. Lett. B 123 (1983) 98.
[25] N. Ushida et al., Phys. Lett. B 206 (1988) 375.
[26] J.D. Richman, P.R. Burchat Rev. Mod. Phys. 67 (1995) 893.
[27] K. Lang et al., Z. Phys. C 33 (1987) 483.
[28] C. Baltay et al., Phys. Rev. Lett. 55 (1985) 2543.
[29] D. Geiregat et al., Phys. Lett. B 245 (1990) 271.
[30] S.R. Mishra et al., Phys. Rev. Lett. 66 (1991) 3117.
[31] F. James, MINUIT 94.1, CERN Program Library Long Writeup D506.
[32] A.J. Buras, K.J.F. Gaemers, Nucl. Phys. B 132 (1978) 249.
[33] G. Atherton et al., CERN 80-07, August 1980. G. Ambrosini et al., Phys. Lett. B 420 (1998) 225; B 425 (1998) 208; Eur. Phys. J. C 10 (1999) 605.